Low-toxicity nanoMolar scaffolds with hundreds of variants generated by computational co-evolution into prokaryotic potassium channel cavities

short title: KcsA co-evolutionary docking

Coll, J*.
*Department of Biotechnology. Centro Nacional INIA-CSIC. Madrid, Spain.
*Julio Coll, orcid: 0000-0001-8496-3493
Email: juliocollm@gmail.com; julio.coll.m@csic.inia.es (JC)
* Corresponding author

Abstract

Human potassium channels (Kir) are implicated in numerous dysfunction diseases genetically affecting cardiovascular, skeletal-muscle and/or synaptic-neuronal functions. Variations in Kir sequences, organ distribution differences and toxicity of some of their known inhibitors, require alternative drugs to interfere specifically with each human Kir molecular species. In this work, a prokaryotic asymmetric transmembrane homotetramer potassium (K^+) channel protein highly homologous to Kirs has been used as their model. Computational methods combining molecular parent co-evolutions confirmed by consensus docking, were explored as possible prove-of-concept to generate rather than screen for numerous KcsA docking-ligands. The explorations of the KcsA central cavity and of their interface lipid-binding shallow-grooves, predicted highly specific novel scaffolds with low-toxicity risks, displaying hundreds of molecular variations of new scaffolds within nanoMolar-ranged affinities. Experimental validation and/or additional computational research on human Kirs could be attempted in the future.

Keywords: Co-evolutionary docking; Consensus docking; KcsA, Kir, Potassium channels

Introduction

Potassium (K^+) channels are asymmetric homotetrameric transmembrane proteins that control K^+-flows across biological cell membranes[1, 2]. In humans, Kirs (**K**$^+$ **i**nwardly **r**ectifying) belong to a family of ~ 400 ion channel genes whose genetic mutations are often implicated in diverse cardiovascular, skeletal muscle or synaptic neuronal functions or channelopathies. Distinct mutations on the Kir-coding genes can affect the electrical excitability [3] of nerve or muscle cells, channel gating, conductance, ion selectivity, and/or signal transduction. Kir channel dysfunctions can lead to i) periodic paralysis and cardiac arrhythmias when targeting the KCNJ2 gene (**KC**ha**N**nel, subfamily **J**, member **2**) as in the Andersen-Tawil Syndrome, ii) alterations of heart electrical activity, causing arrhythmias and sudden cardiac death when targeting KCNQ1, as in the Long QT Syndrome, iii) episodes of lack of coordination when targeting KCNA1 as in Episodic Ataxia[4], iv) ventricular arrhythmias causing sudden cardiac death, when targeting KCNH2, as in the short QT Syndrome, and other channelopathies[5-7] as well as some new that may be discovered in future research.

The bacterial **K**$^+$ **c**hannel from ***S**treptomyces livid**a**ns* (KcsA) is one of the most widely used model for the homologous human Kir channels [8]. KcsA is an homotetramer protein of 160 amino acids assembled in 4 transmembrane α-helices per monomer. According to the crystallographic structure of its 124 amino acid transmembrane fragment [9], KcsA contains the four monomers packed asymmetrically around a central hydrophilic pore that serves for the K^+ flow (**Figure 1C, top view**). Its N and C-terminal sequences face the intracellular cytoplasm. Although less studied than the transmembrane α-helices, KcsA C-terminal sequences have been also implicated in controlling the K^+ flow [10, 11]. The KcsA transmembrane α-helices form an inverted truncated V cone accommodating ion selectivity filters at their extracellular top at the mouth of the cone[12]. Such ion selectivity filters contain 4 K^+ binding sites of four highly conserved copies of ^{75}TVGYG stretches that provide closed / open reversible conformations to stop / allow K^+ flows (**Figure 1AB, green sticks**).

Often used as disinfectants, **q**uaternary-**a**mmonium **c**ompounds (qac) displaying one positively charged Nitrogen atom (N^+)[13] at their centre, strongly inhibit K^+ channel flows by competing with the channel K^+ -binding selectivity filters [13-16]. Symmetrical alkyl-chain qac derivatives of different lengths (i.e, tetraethylammonium) discovered additional hydrophobic cavities for binding which extended the central qac-binding cavity towards the four monomeric interfaces[15]. Alkyl-qac binds both to the channel internal hydrophilic cavities below the K^+ selectivity filters such as ^{100}I and ^{103}F amino acid side chains stabilizing qac binding [13, 14, 17], increasing K^+ loss, and inactivating ion channels. These results suggested that non-toxic qac alternatives (i.e., other hydrophilic heads and/or other hydrophobic alkyl chains) might predict higher affinities and more potent inhibitors..

Although alkyl-qac are potent *in vitro* inhibitors, they are not viable as therapeutic drugs because of their high toxicity risks at the concentrations required for therapeutic efficacy. Furthermore, symmetric alkyl-qac lack specificity to human Kir molecular species of particular physiological functions (targeting multiple Kir channels and/or physiological off-targets should be avoided) and have shown pharmacokinetic limitations including reduced absorption, distribution, metabolism, and/or excretion.

Anionic lipids / phospholipids [18, 19, 20] have been implicated also in the structure / function of K^+ channels, despite crystallographic diacyl-glycerol (dga) being the first and most detected lipid (i.e., 1k4c). This and/or other lipid fragment(s) detected in crystallographic structures occupy four surface shallow-grooves outside of the annular centre of the homotetramer. Interactions of lipid hydrophilic heads with arginine residues from two contiguous monomers (^{64}R and ^{89}R) are most probably implicated in the crystallographically detected interactions[21]. It may be possible that specific lipids could optimize KcsA channel assembly and/or function[8, 19, 22], since for instance, KcsA binds phosphatidylglycerol better than phosphatidylcholine[9, 20, 23]. Briefly, four anionic lipids bind KcsA at the four interfaces of each of two adjacent KcsA monomers in surface shallow-grooves per monomer (**Figure 1ABC, red spheres**), suggesting that lipid hydrophilic heads and/or their alkyl-chains may allosterically influence K^+ flows.

Alternative human drug anti-Kir channel intensive searches are on going worldwide focused on particular channelopathies. Some of these examples are trying to identify highly specific and more potent drug-like compounds to target defined human Kir channels, including repurposing of approved drugs. Public examples of approved drugs presently being tested to control human channelopathies are for instance, Retigabine (tested as antiepileptic drug [23-25]), Dofetilide (tested as antiarrhythmic for atrial fibrillation[26-29], and Senicapoc (tested against ischemic stroke [30] despite showing off-target effects [31]). Future research may lead to new discoverings in the anti-channelopathies research field, but progress is slow mostly due to the small amount of drug-like compound alternatives and to the extensive clinical tests required for each possibility.

Generation rather than screening, were employed in this work to search for new anti-KcsA ligand candidates using the ***D**ata**W**arrior **B**uild **E**volutionary **L**ibrary* (DW-BEL) algorithms[2-5]. Starting from defined parent molecules and their preliminarily identified docking cavity, DW-BEL co-evolution generated tens of thousands raw children and thousands of highly specific cavity-fitting children molecules [2-5,32] selected by their docking affinities. Despite the particular toxicity and/or steric difficulties found when targeting the known KcsA central cavity and/or lipid surfaces, respectively, the random generation of children molecules was very successful. By restricting their molecular weight, hydrophobicity [6, 7, 8-11] and toxicity risks and quantitating their affinities by the most accurate **A**uto**D**ock**V**ina (ADV) program[33], thousands of low toxicity, high specificity and sub-nanoMolar computational children predictions were identified. Further co-evolutions and deeper preference criteria could be applied, for instance by designing other parent molecules and/or by increasing computer memories since the vast chemical space limits have not yet been reached. In the absence of any experimental confirmatory data, all these predicted docking-cavities and new ligand candidates remain hypothetical.

A selection of top-children and ther properties were included as **Supplementary Material**. Tables were provided with selection sliders to simultaneously apply multiple alternative criteria.

Computational Methods

Generation of rather than screening for KcsA ligands

The **D**ata**W**arrior-**B**uild **E**volutionary **L**ibrary (DW-BEL) algorithms were employed to generate tens of thousands of raw unique children from one parent molecule and select those fitting an initial protein-ligand cavity (fitted-children). The Java's DW program was updated for Windows as described before (**Table S1**)[34, 35] including some modifications to adapt to large number of runs. The initial parent molecules were selected from previously proposed KcsA ligands such as **q**uaternary-**a**mmonium **c**ompounds (qac)[14], **d**iacyl-**g**lycerol (dga)[9] or user-designed pseudoligands. Fine-tuning of possible alternatives were introduced by optimizing less-toxic derivatives (i.e., substituting the central N^+ by C in qac compounds), restricting parts of the initial parent molecules with the DW-BEL lazo option (i.e., head of lipids or hydrophobic alkyl chains) or introducing pseudoligands by PyMol elongation of alkyl-chains.

The docking cavities for DW-BEL defined by pre-docked protein-ligand complexes coded in *.pdb files, provided an starting minimal docking cavity. During co-evolution, each particular fitted-children adapted to ±10 Å cavity flexibilities.

Co-evolution proceeded according to user-defined criteria consisting in both preferences and relative 1-4 weights. The criteria were, minimal DW docking-scores with relative weight 4 (to maximize docking affinities using the optimal force-field mmff94s+ algorithm[37]), molecular weight <= 600 g/mol with relative weight 2 and cLog <=8 with relative weight 1 (to limit children unspecificities) and Toxicity risk <=1 with relative weight 4 (to reduce hundreds of toxicity risks and/or nasty functions during co-evolution). Because computer memory limitations, the maximal number of consecutive runs were limited to 3, but after 24 hours or when reaching RAM >100 Gb, runs were manually stopped. The resulting DW output docking-scores of the fitted-children were expressed in negative unitless values (the more negative, the higher affinity).

To prepare for consensus or confirmatory docking, the DW-BEL resulting fitted-children were filtered to exclude any remaining toxicities and/or nasty functions to yield non-toxic fitted-children. A DW macro filter[33] including hundreds of mutagenesis, tumorigenicity, reproductive interference and irritant molecular signatures, and/or nasty functions was designed for these purposes [35]. The non-toxic fitted-children were DW saved as special 3D *.sdf files using previously described options including mmff94s+ minimization[37]. Such saving methods were critically required to preserve their 2D geometries [32] for PyMol visualization (split_states PyMol command)[34] and/or for optimal ADV re-docking.

Confirmation by AutoDockVina (ADV) docking

The **A**uto**D**ock**V**ina (ADV) [46] program included into the PyRx-0.98/1.0 Python package, was modified to large scale docking [36]. The ADV data was required for consensus or confirmation of the DW-BEL affinities, quantification in ~ nM affinities and generation of detailed 3D docked complexes for PyMol visual inspection[34, 37-39]. Briefly, non-toxic fitted-children saved as special 3D *sdf files were minimized and converted to *.pdbqt files[40] using the mmff94s (Merck) force-field option. A grid of 45x45x45 Å automatically centered around the corresponding PyMol / centerofmass was designed for ADV docking for each of the KcsA protein targets (each grid-box used can be visualized at the corresponding **Supplementary Material**). ADV docking of thousands of non-toxic fitted-children lasted during several days depending on the cavity and the size of their children molecules. The ADV docking-score output results were delivered by the program in - Kcal/mol[41, 38, 42, 43] and converted to ~ nM affinities by the formula, $10^{9*}(\exp^{(Kcal/mol/0.592)})$.

Computational improvements and programs used

Table 1
Software, computational improvements and hardware for computational manipulations

name	version	Main use and references	url
DataWarrior	Updated 5.5.0 Windows/Linus	Evolutionary docking[34] Commercial ChemSpace	https://openmolecules.org/ datawarrior/download.html)
Toxicity & nasty macro	2023	Eliminate toxic / nastic fitted-children after co-evolution[44]	
Toxicity Risks	2023 Updated DataWarrior	Minimize toxic / nasty raw-children during co-evolution[35]	https://openmolecules.org/ datawarrior/download.html)
Babel & AutoDockVina	Home-adapted PyRx 098/1.0	Mmff94s minimization[49] & 2D conservation	https://pyrx.sourceforge.io/
ADV consensus	2023	Anti-bacterial cell division[34, 45]	
2D geometry conservation	2023	DW saving-SD files with mmff94s+ for ADV docking[57]	
MolSoft	3.9 Win64bit	Manipulation of sdf files	https://www.molsoft.com/download.html
PyMol	2.5.7.	Visualization of molecules	https://www.pymol.org/
DiscoveryStudio	21.1.1.0.20298	Visualization of 2D molecules	https://discover.3ds.com/discovery-studio-visualizer-download
OriginPro	2022	Calculations and Figures	https://www.originlab.com/
Pseudoligands	2023	Pseudoligand parents[32]	
LigPlus+	2.2.8.	Amino acid bonds[34]	https://www.ebi.ac.uk/thornton--rv/software/LigPlus/ applicence.html
AMD Ryzen i9 computer	4 DDR4 x 32 Gb memory[32]	47 CPU hardware	https://www.pcspecialist.es/

Results

Strategy to generate large numbers of KcsA fitted-children

Different parent molecules, predicted cavities targeted by the docked parent and optimal co-evolution criteria were optimized to generate thousands of fitted-children by DW-BEL. To increase their prediction accuracies, to quantitate their docking-scores and to confirm their targeted cavities in the presence of wider cavity competitors, one additional ADV docking step followed.

The KcsA 1k4c homotetramer model was chosen to apply DW-BEL and subsequent ADV, because it codes for the open-state that favors K^+ flow and also have shown to be an inhibitor target. To begin our explorations, two previously proposed binding sites were chosen on the 1k4c model, **i)** the central cavity below the ion-sensitivity filter, targeted by alkyl-qac inhibitors (**Figure 1C, central blue sphere**) and **ii)** the four lipid shallow-grooves of monomer interfaces formed by the external surface of the homotetramer (**Figure 1ABC, red spheres**).

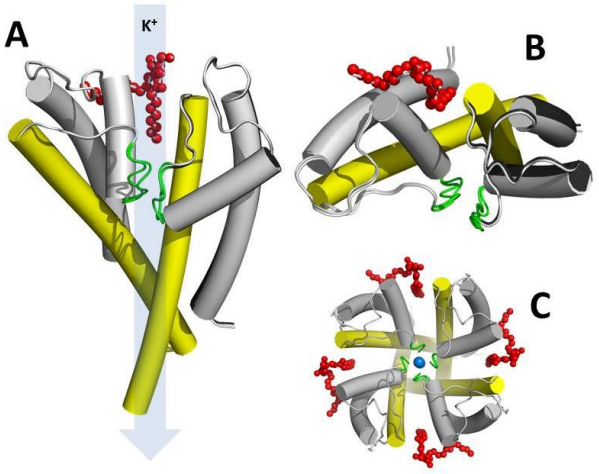

Figure 1
Scheme of two KcsA monomers of the tetramer (12-124 amino acids per monomer) forming one asymmetric dimer: side-view (A) and top-view (B) and homotetramer top-view (C)
Only 2 KcsA monomers (**AB**) of the homotetrameric 1k4c (**C**) were represented for clarity. Transmembrane α-helices hold the homotetramer into the cellular membrane forming a central hydrophilic pore (**C**). The extracellular environment is up and the intracellular cytoplasm is down (**A**). Two dimer images, one from the open conformation at high K^+ (**1k4c.**pdb) and other from the closed conformation at low K^+ (**1k4d.**pdb), were merged to visualize their differences at their ion-selectivity filters (**green cartoon lines**).
A cartoon cylinders, side-view of 1k4c+1k4d merged homodimers.
B cartoon cylinders, top-view of 1k4c+1k4d merged homodimers
C cartoon cylinders, top-view of the 1k4c homotetramer.
Yellow cylinders, transmembrane α-helices expanding residues 86-124.
Red spheres, diacyl-glycerol of 1k4c behind the ion selectivity filters
Green cartoon lines, 1k4c+1k4d ion-selectivity filters merging the K^+ binding ^{75}TVGIT amino acid sequences
Blue vertical background arrow (A), Scheme of the K^+ flow through the hydrophilic pore when opened
Central blue sphere (C), K^+ at the center of the 1k4c hydrophilic pore (channel)

Targeting the central cavity

The KcsA central cavity and its hydrophobic lateral extensions were first targeted by DW-BEL co-evolution with several alkyl-qac of known *in vitro* inhibitory activities [14] (tetrabutylammonium, tetrahexylammonium, tetraoctylammonium). However, most of the randomly generated fitted-children were eliminated by the DW-BEL toxicity and nasty function algorithms during co-evolution and/or eliminated by the macro filter after co-evolution . Since their toxicity risk identifications were mostly due to their central N^+ atom, substitution of N^+ by one Carbon atom (qcc alternatives), were attempted which resulted in successful generation of DW-BEL non-toxic alternatives. One qcc symmetric molecule which was a non-toxic star-like molecule containing a central Carbon with 4 arms of 4 Carbons, each linked to a terminal Gly, here called 4x4Gly (**C25H48N4O8** formula) (**Figure 2, 2D right image**), was optimized by co-evolution from parents with different C-chain lengths (data not shown). DW-BEL co-evolution from the 4x4Gly parent predicted 2776 non-toxic fitted-children to the KcsA 1k4c central cavity (**Table S1**). Their affinity predictions were confirmed by exceptional high correlations with those from ADV (**Figure 2**). For instance, the top-child number 7810 predicted ~ 0.1 nM docking affinity (**Figure 2, red open circles**), in contrast to ~ 1 µM of its 4x4Gly parent or to the toxic tetraoctylammonium inhibitor (**Figure 2, solid and crossed green circles,** respectively). The 6-ring 7810 top-child scaffold (**Figure 5**) was the most representative scaffold among the non-toxic fitted-children. Ten top-children data corresponding to **Figure 2**, were listed in **Table S2** to visualize some of their properties. Complete data for 100 top-children were also supplied as **Supporting Materials** (**100top-children.centralcavity.dwar** and ***.pse**).

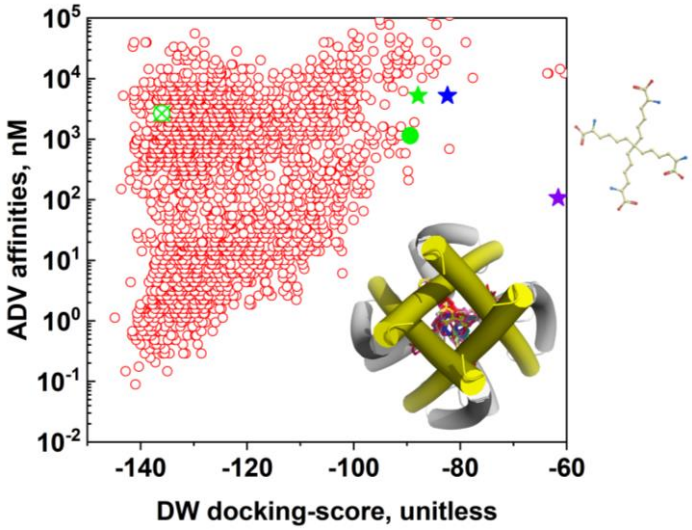

Figure 2
ADV *vs* DW-BEL non-toxic fitted-children targeting the homotetramer central-cavity
DW-BEL were tested at molecular weights of < 650, 600, 500, or 300 g/mol. Only the fitted-children predicted at <300 g/mol were represented. **Up-right structure**, 2D scheme of the 4x4Gly non-toxic parent.
Down-right cartoon, bottom-view of the 1k4c homotetramer. **Yellow cylinders**, transmembrane α-helices (residues 68-124). **Down-right Multicolor sticks**, top-children docked to the central cavity.
Red open circles, 2776 fitted-children. **Green circle**, non-toxic 4x4Gly parent
Green crossed, tetraoctylammonium qac inhibitor (TOA, pubchem ID 2734117).
Green star, Dofetilide. **Blue star**, Dibutilide. **Purple star**, Senicapoc.
Visualization of complexes with 1k4c at **Supporting Materials / ChannelLigandsOnResearch.pse.**

Targeting the lipid-surface shallow-groove

Co-evolutions were then attempted using diacyl glycerol (dga) as the parent to target one of the lipid-surface shallow-grooves at the crystallographic 1k4c homotetramer model (**Figure 1C, red spheres**). However, although hundreds of raw-children could be generated, the DW-BEL program shortly stopped without predicting any fitted-children. Results were similar despite testing many alternative criteria combinations (**Table S1, homotetramer lipid cavity**). Apparently the dga head defined a limited cavity to allow for DW-BEL selection of any fitted-children. Because one cavity was *sine-qua-non* requirement for DW-BEL co-evolution, one hypothetical 1k4c homoctamer could be a possible alternative. Therefore, one 1k4c hypothetical homoctamer forming a PyMol visible cavity for dga was constructed using their supplied crystallographic symmetry coordinates (**Figure 3, down-right cartoon**). In contrast to the homotetramer, DW-BEL from the dga parent targeting the homoctamer-dga complex, generated 52824 random-raw-children, of which 3891 (~ 7 %) were predicted as non-toxic fitted-children (**Table S1, raw- and NTNV-children**). These non-toxic fitted-children predicted exceptionally high correlations between DW-BEL and ADV affinity estimations, most of them at higher affinities than its dga parent (**Figure 3, red circles** *vs* **green circle**). For instance, the top-child number 34511 predicted ~ 0.05 nM affinity, compared to ~ 30 µM of its dga parent (**Figure 3, red circles** *vs* **green circle**) and was the most representative scaffold among the top-children (96 %, n=100) including additions and alternative atoms, bonds / bond types and/or rings / ring numbers. To note that all these non-toxic fitted-children targeted similar homoctamer hypothetical lipid cavities, despite the many other possibilities offered by the wider 45x45x45 Å grid which included 2 center cavities among many other possibilities **(Supporting Materials / 100top-children.lipidcavity.pse).** Ten top-children data were listed in **Table S1** to visualize some of their properties. Additionally, 100 children data were supplied as DW Tables provided with sliders including DW-BEL and ADV affinities, molecular weight and hydrophobic properties (**Supporting Materials / 100top-children.lipidcavity.dwar**).

Targeting the homoctamer lipid cavity with elongated alkyl-chain parent

Because the previous dga parent did not randomly generated non-toxic fitted-children with any of the long alkyl-chains characteristic of natural lipid molecules, a two-step strategy to explore such possibilities was designed. For the heads-only first step, dga co-evolutions were made by maintaining its alkyl-chains constant, and varying their heads. For the alkyl-only second step, the best top-head non-toxic fitted-child predicted from the first step, was maintained constant while their alkyl-chains were DW-BEL varied into their grandchildren.

These heads-only co-evolutions, predicted 3891 non-toxic fitted-children with higher affinities than their dga parent (**Figure 4, gray circles** *vs* **green circle**). However, few non-toxic fitted-children predicted affinities < 100 nM, in contrast to those predicted when using the whole dga molecule as parent (**Figure 3**). Nevertheless, the best top-child number 20900 was chosen as the parent (~250 nM) for the second step of alkyl-only co-evolutions.

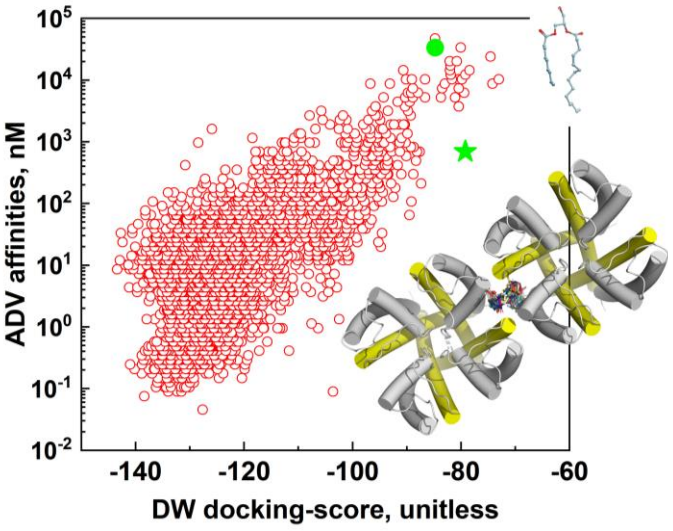

Figure 3
ADV vs DW-BEL non-toxic fitted-children targeting the homoctamer lipid-cavity
Up-right structure, dga from the 1k4c model [9] **Down-right cartoon**, KcsA homoctamer.
Yellow cylinders, transmembrane α-helices.
Multicolor sticks, top-children at the lipid cavity (Down-right).
Red open circles, 3892 fitted-children. **Green circle**, dga. **Green star**, Retigabine (**Supporting Materials**).

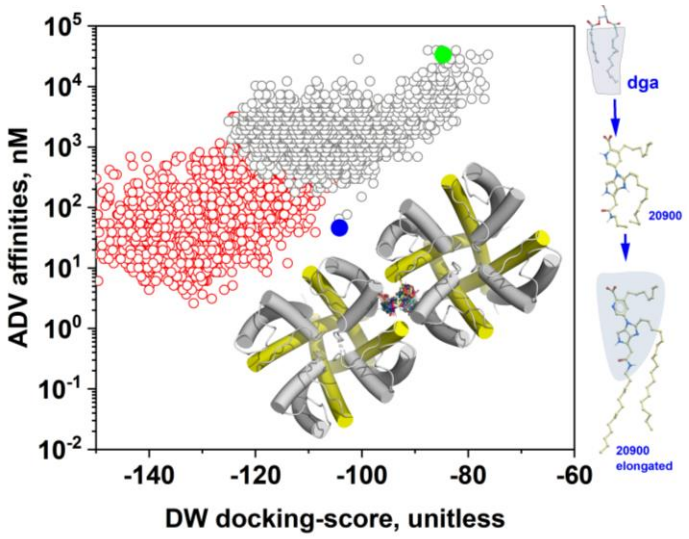

Figure 4
ADV *vs* DW-BEL non-toxic fitted children targeting elongated cavities
ADV vs DW-BEL non-toxic fitted-children generated by co-evolution from the dga parent with constant alkyl chains (up-right) or ADV vs DW-BEL non-toxic fitted grandchildren generated by co-evolution from top-child head group and evolved alkyl chains (down right) targeting the KcsA homoctamer lipid-interface cavity,
Up-right, dga from the 1k4c model [9] parent maintaining constant the acyl chains
Down-right, top-children 20900 parent maintaining constant the top-child head generated first
Shadows at the molecular structures. Part of the parent molecules maintained constant during evolution.
Cartoon down-right, KcsA homoctamer.. **Yellow cylinders**, longer transmembrane α-helices.
Multicolor sticks, grandchildren at the elongated cavity (Down-right).
Blue circle, dga parent co-evolved with constant alkyl chains
Green circle, child co-evolved parent with constant head
Gray open circles, dga head-only children
Red circles, 20900 alkyl-only fitted-grandchildren.

To perform the alkyl-only co-evolutions, a pseudoligand parent was constructed in PyMol from top-child 20900 by elongating its alkyl-chains downward the homoctamer interface to extend its cavity (**Figure S1B, red spheres**). Furthermore, DW-BEL molecular weight preference criteria were increased from < 600 to < 900 g/mol. The alkyl-only co-evolutions, predicted 2374 fitted-grandchildren. However, only ~ half of the non-toxic fitted-grandchildren predicted higher affinities than their 20900 parent (**Figure 4, red circles** *vs* **blue circle**). Furthermore, correlations with their ADV affinity estimations extended for a lower range than those predicted when using the whole dga molecule as parent (**Figure 3**). Nevertheless, the top-grandchild with the most abundant scaffold was number 20346 predicting affinities of ~ 4 nM (**Table S2** and **Figure 4, red circles**), compared to the ~ 250 nM of its 20900 parent (**Figure 4, blue circle**). The 6-ring

20346 top-grandchild scaffold (**Figure 5**) was the most representative scaffold among the non-toxic fitted-grandchildren. Ten top-grandchildren data were listed in **Table S1** and 100 top-grand children were supplied as **Supporting Materials** (**100top-grandchildren.elongatedcavity.dwar** and ***.pse**).

Comparative study of representative top-children targeting central, lipid and elongated cavities

It was remarkable that targeting central, lipid or elongated 1k4c cavities, only one dominant scaffold was predicted for each of those cavities (representative top-child scaffold) (**Figure 5, Table S1**). It was also remarkable that despite the many peripheral atom variations for each dominant scaffold, most of the 100 top-children targeted similar docking cavities than their corresponding parents (**Supplementary Material /*.pse**). Some critical interactions between the top non-toxic fitted-children representatives and the amino acids at the KcsA chains included previously described amino acid contact in several chains. For example, the ^{64}R and ^{89}R implicated before in lipid head interactions (**Table S3, red numbers**), the ^{75}T of the K^+ binding ^{75}TVGYG sequence (**Table S3, green numbers**) and/or the inner α-helix ^{100}I and ^{103}F residues known to stabilize qac binding (**Table S3, blue numbers**). There were also other amino acids implicated in the elongated cavity that were not targeted by the other ligands. Nevertheless, despite having longer alkyl-chains, most of the elongated non-toxic fitted-grandchildren predicted 10-100-fold lower affinities than those evolved by targeting the central or the lipid cavities (Compare affinity values of **Figure 2** and **3** with **4**).

K^+ channel ligands from ongoing research

Dofetilide / Dibutilide, Senicapoc and Retigabine were DW and ADV docked to the homoctamer model. Despite including both central and lipid cavities into the ADV 45x45x45 Å grid, the results predicted that Dofetilide / Dibutilide and Senicapoc preferred any of the central cavities. In contrast Retigabine remained into the initial lipid cavity (**Supporting Materials / ChannelLigandsOnResearch.pse**). Comparison of ADV *vs* DW profiles of Dofetilide / Dibutilide and Senicapoc (**Figure 2, green, blue, purple stars**) and Retigabine (**Figure 3, green star**) data with the non-toxic fitted-children candidates described here predict that none of these research on-going molecules predicted higher affinities than most of the children candidate alternatives proposed here.

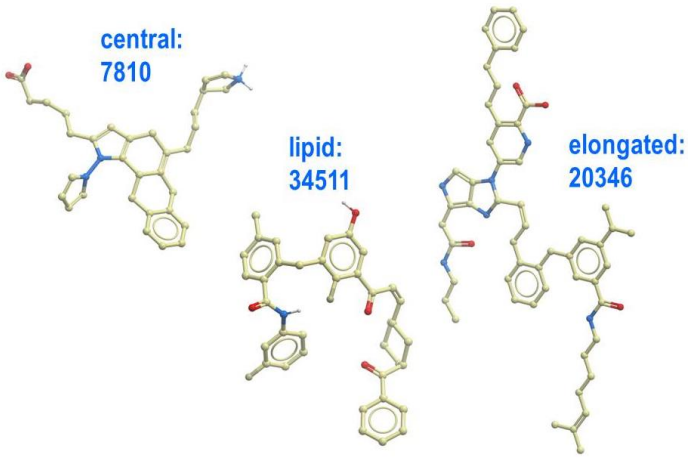

Figure 5
Representative non-toxic fitted-child / -grandchild scaffolds
The representatives were drawn in MolSoft. More molecular details in **Table S1** and **Supplementary Material**
Red spheres, Oxygens. **Blue spheres**, Nitrogens. **Light green spheres and sticks**, Carbons and bonds.
7810, top-child predicting docking to the central cavity (**Figure 2**).
34511 top-child predicting docking to the lipid cavity (**Figure 3**).
20346 top-grandchild predicting docking to the elongated cavity (**Figure 4**).

Discussion

To computationally explore alternative ligands to the prokaryotic KcsA 1k4c model, a "generating rather than screening" strategy has been developed. The differences between these two types of strategies could be compared to those between going for submarine fishing or waiting for the fish to pass by (submarine-pursuing rather than wait-fishing). To explore such strategy, DW-BEL co-evolutions generating thousands of fitted-children have been combined with ADV affinity consensus to improve predictions accuracies. Among other achievements, some of the results surprisingly predicted high correlations and similar docking-cavities between the two docking programs despite their different algorithms and software languages (python and java), something that could not be reported so clearly in several previous co-evolution studies with other protein /ligand pairs[48, 58, 46, 44, 35].

The central homotetramer and the homoctamer lipid cavities successfully generated thousands of non-toxic fitted-children. Their top-children predicted low nanoMolar affinities, high specificities and similar docking cavities than previously described qac or lipid binding molecules. Some of these top-children, targeting similar binding cavities that previously demonstrate inhibitors may increase their possibilities to real bindings and perhaps to experimentally interfere with KcsA K^+ flows. In contrast, lower affinities and therefore much lower expectatives, were predicted by children derived from elongated dga-parents.

One dominant scaffold with the higher affinities were predicted to each of the best targeted central and lipid cavities, each one of them with hundreds of atom variations. To identify which one of those will show experimental anti-channel activities, there are no other computational methods. We are assuming that those with the higher affinities, would have more probabilities to bind. However, there are no evidences that the higher affinities will have better binding properties than some other with lower affinity. Furthermore, the strategies explored here only identified an small number of scaffold possibilities. The chemical space has many other that remain unexplored.

As mentioned above, there were hundreds of alternative children, in contrast to those predicted by more traditional screening of chemical banks. Such amount of alternatives could allow to rapidly screen all the different alphafold human Kir sequences to select for those specific for each of the human Kir variants. Additionally, large numbers of candidates could be used to extract those computationally recognizing known mutations, molecular target variations, and/or off-targets, etc. Something similar was employed with other protein /ligand pair examples for instance to select anticoagulants affecting both rats and their resistant mutants but not humans[46] or monkeypox Tecovirimat-resistant variants [32].

We have applied here several improvements to the DW-BEL and ADV algorithms that were incorporated step-by-step during the last months into different protein / ligand pair models [48, 58, 46, 44, 35]. However, deeper explorations of lower molecular weight targets, targeting the C-terminal KcsA ,together with the screening of sequence-specific homologous cavities of all human Kir variants, would demand higher computer memories to best penetrate into the vast chemical space to increase the probabilities to identify drug-like molecules[38, 39].

In conclusion, using homotetramer and homoctamer-derived crystallographic models, top-children ligand molecules could be predicted to the 1k4c central and lipid cavities. The top-children predicted high:

i) DW-ADV correlations,
ii) Low nanoMolar range affinities,
iii) Few scaffolds and hundreds of drug-like candidates.

Supporting Materials

- 100top-children.centralcavity.dwar. These *.dwar *DW* tables contain 100 top-children selected by their ADV affinity estimations (**Figure 2**). Tables are provided with threshold slider-filters to their DW and ADV docking-scores, Molecular weights and clogP properties to select particular threshold combinations. The *.dwar files can be opened in DW freely available at https://openmolecules.org/datawarrior/download.htm.

- 100top-children.lipidcavity.dwar. These *.dwar *DW* tables contain 100 top-children selected by their ADV affinity estimations (**Figure 3**). Tables are provided with threshold slider-filters to their DW and ADV docking-scores, Molecular weights and clogP properties to select particular threshold combinations. The *.dwar files can be opened in DW freely available at https://openmolecules.org/datawarrior/download.htm.

- 100top-children.elongatedcavity.dwar. These *.dwar *DW* tables contain 100 top-children selected by their ADV affinity estimations (**Figure 4**). Tables are provided with threshold slider-filters to their DW and ADV docking-scores, Molecular weights and clogP properties to select particular threshold combinations. The *.dwar files can be opened in DW freely available at https://openmolecules.org/datawarrior/download.htm.

- **100top-children.centralcavity.pse**. The 100 top-children ADV complexes (ordered by nM affinities) with the homotetramer AcsA model to be visualized in PyMol vs2.5.3.

- **100top-children.lipidcavity.pse**. The 100 top-children ADV complexes (ordered by nM affinities) with the A homoctamer AcsA model to be visualized in PyMol vs2.5.3.

- **100top-children.elongatedcavity1.pse**. The 100 top-children ADV complexes (ordered by nM affinities) with the A homoctamer AcsA model to be visualized in PyMol vs2.5.3.

KchannelLigandsOnResearch.pse . Docking of Dofetilide / Dibutilide and Senicapoc (**Figure 2, green, blue, purple stars**) and Retigabine (**Figure 3, green star**) to the hypothetical homoctamer 1k4c.

Supplementary information

Table S1
***DW-BEL* co-evolutions of representative top-children**

KcsA Homo-Target	parent	cavity	Raw-children	Fitted-children	NTN-children	%	Top-child, ID
Tetramer	**4x4Gly**	central	35315	3096	2775	7.8	7810
Tetramer	**Dga**	Lipid	784	0	0	0	none
Octamer	**Dga**	Lipid	52824	4397	3891	7.3	34511
Octamer	**Dga**	Elongated	33101	2821	2373	7.1	20346

DW-BEL co-evolution user-criteria: Toxicity Risk <=1 (weight = 4), Docking Score (4), Molecular weight <=300 or 600 g/mol (2), and clogP <=4 (1). The fitted-children were filtered by the NTN DW macro to eliminate remaining fitted-children predicting toxicities and nasty functions.
Raw-children, generated children from parent by Java's random Mutator.
Fitted-children, number of children fitting the user-set criteria mentioned above
NTN-children, number of children without remaining toxicities and nasty functions after NTN DW macro
%, calculated by the formula, 100 x NTN children / Number of raw children.

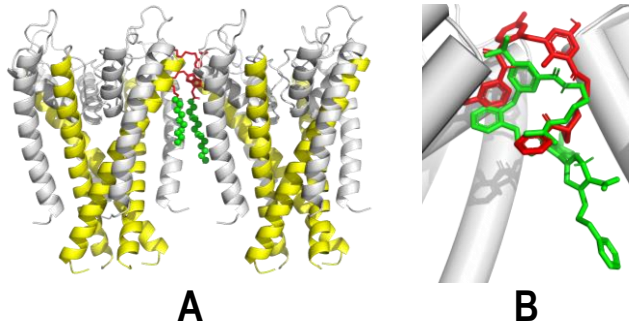

Figure S1
Scheme of the pseudoligand designed by elongation of 20900 docked to the homoctamer (A) and comparison between top-child of Figure 3 (red) and Figure 4 (green)
Carbon atoms of the 20900 top-children were elongated downwards to fill out ~ half of the transmembrane hydrophobic α-helices to design a pseudoligand.
A) Gray cartoons and cylinders, homoctamers using cylinder representations for α-helices
Yellow cylinders, transmembrane α-helices of the 8 x 1k4c monomers
Red sticks, the atoms and bonds of the top-child derived from dga with constant alkyl chains.
Green spheres, Carbon atoms added to the top-head in PyMol
B) Red sticks, lipid top-child 34511. **Green sticks,** elongated top-child 20346.
Gray cartoons and cylinders, slab of two surrounding adjacent KcsA monomers

Table S2
Molecular and docking properties of 10 representative top-scaffolds

ID	MW	LogP	ADV Kcal/mol	ADV nM	DW score	Scaffold X
Central-cavity children						
7810	493	3.0	-13.7	0.09	-140.9	X
15983	509	3.8	-13.4	0.15	-142.7	
6069	492	3.8	-13.4	0.15	-134.9	X
5615	509	3.7	-13.3	0.18	-140.3	X
6383	496	3.8	-13.2	0.21	-137.2	X
5583	495	3.3	-13.1	0.25	-138.1	X
3910	495	2.5	-13.0	0.29	-131.5	X
4059	497	3.6	-13.0	0.29	-139.1	X
4495	497	3.3	-13.0	0.29	-134.5	X
5074	495	3.3	-13.0	0.29	-135.8	X
Lipid-cavity children						
34511	593	7.5	-14.1	0.05	-127.6	X
35150	606	7.0	-13.8	0.08	-138.3	X
45551	602	7.5	-13.7	0.09	-131.5	
37156	607	5.9	-13.7	0.09	-132.3	X
36595	590	7.6	-13.7	0.09	-133.9	X
33309	594	6.6	-13.7	0.09	-103.5	X
31816	596	7.5	-13.6	0.11	-134.5	X
31985	594	7.0	-13.6	0.11	-136.2	X
32920	592	7.3	-13.6	0.11	-130.0	X
32964	580	6.8	-13.6	0.11	-131.5	X
Elongated-cavity grandchildren						
18603	835	8.0	-11.7	2.61	-131.6	
18661	871	7.6	-11.6	3.09	-128.2	
20346	850	8.2	-11.5	3.66	-133.0	X
28370	824	6.8	-11.5	3.66	-129.9	X
24404	824	6.6	-11.4	4.33	-131.9	
26923	856	7.0	-11.4	4.33	-140.0	X
31601	867	6.8	-11.4	4.33	-133.6	
18646	851	8.4	-11.4	4.33	-125.8	X
22213	874	7.6	-11.3	5.13	-130.8	X
31142	885	6.3	-11.3	5.13	-154.8	X

Supporting Materials included the corresponding 100 top-children or -grandchildren files. Tables provided with threshold slider-filters including 2D structures, DW-BEL and ADV docking-scores and affinities, Molecular weights and Hydophobic logP properties.
X, same scaffolds than their corresponding top-child or -grandchild (**green background**).
Supplementary Material / 100top-children or top-grandchildren ....dwar files visualize the scaffolds and properties of the 100 tops .
Green background, representative top-child scaffold (Figure 5).

Table S3
KcsA amino acids around 4 Å of representative tops

Chains	/Positions		Amino acids	4x4Gly	7810	dga	34511	20346
A	33	T	Thr					
	36	L	Leu					
	37	V	Val					
	40	L	Leu					
	41	L	Leu					
	63	P	Pro					
	64	R	Arg*					
	66	L	Leu					
	67	W	Trp					
	70	V	Val					
	73	A	Ala	H				
	74	T	Thr					
	*75	T	Thr					
	99	G	Gly					
	*100	I	Ile					
	102	S	Ser		H			
	*103	F	Phe					
	106	V	Val					
B	36	L	Leu					
	73	A	Ala					
	74	T	Thr					
	*75	T	Thr					
	99	G	Gly					
	*100	I	Ile					
	102	S	Ser					
	*103	F	Phe					
C	73	A	Ala	H				
	74	T	Thr					
	*75	T	Thr					
	85	T	Thr					
	86	L	Leu					
	87	W	Trp					
	89	R	Arg*					
	90	C	Cys					
	91	V	Val					
	93	V	Val					
	94	V	Val					
	97	V	Val					
	99	G	Gly					
	*100	I	Ile					
	*103	F	Phe					
	193	V	Val					
D	*75	T	Thr					
	*100	I	Ile					
G	85	T	Thr					
	86	L	Leu					
	87	W	Trp			H		
	89	R	Arg*				H	
H	62	Y	Tyr					
	63	P	Pro					
	64	R	Arg*			H		
	66	L	Leu					
	67	W	Trp					

Chains, A to H. (ABCDEFGH). **Positions**, KcsA amino acid sequence
red numbers* , Arg proposed to bind head lipids
***green numbers,** amino acids participating in K^+ binding (^{75}TVGYG)
***blue numbers**, qac hydrophobic interactions with some inner helix residues
Blue and yellow rectangle backgrounds, residues predicted at 4 Å to ligands and top-children atoms (LigPlus/LigPlot).
Yellow backgrounds, parents
H, LigPlus/LigPlot predicted Hydrogen bonds.

Funding
The work was carried out without any external financial contribution

Competing interests
The author declares no competing interests

Authors' contributions
JC designed, performed and analyzed the dockings and drafted the manuscript.

Acknowledgements
Thanks are specially due to N.Behrnd of Idorsia Pharmaceuticals Ltd. at Allschwil (Switzerland) for help to develop the NTN DW macro and discussions on 2D structure conservation issues in and out of the DW forum. Thanks are also due to Dr. A. Villena from the University of Leon (Spain) for bibliographic references.

References

[1]Brelidze, T.I. Heteromeric wild-type/mutant potassium channel subunit composition as a major determinant of channelopathy phenotype in heterozygous patients.*J Gen Physiol.* 2023, 155: http://dx.doi.org/10.1085/jgp.202313333.
[2]Inoue, M., *et al.* TASK channels: channelopathies, trafficking, and receptor-mediated inhibition.*Pflugers Arch.* 2020, 472: 911-922 http://dx.doi.org/10.1007/s00424-020-02403-3.
[3]Hamilton, M.J. and Suri, M. "Electrifying dysmorphology": Potassium channelopathies causing dysmorphic syndromes.*Adv Genet.* 2020, 105: 137-174 http://dx.doi.org/10.1016/bs.adgen.2020.03.002.
[4]Gazulla, J. and Berciano, J. Potential Benefit of Channel Activators in Loss-of-Function Primary Potassium Channelopathies Causing Heredoataxia.*Cerebellum.* 2023: http://dx.doi.org/10.1007/s12311-023-01584-8.

[5]Kumar, M. and Pattnaik, B.R. Focus on Kir7.1: physiology and channelopathy.*Channels (Austin).* 2014, 8: 488-95 http://dx.doi.org/10.4161/19336950.2014.959809.
[6]Gribkoff, V.K. and Winquist, R.J. Potassium channelopathies associated with epilepsy-related syndromes and directions for therapeutic intervention.*Biochem Pharmacol.* 2023, 208: 115413 http://dx.doi.org/10.1016/j.bcp.2023.115413.
[7]Gripp, K.W., *et al.* Syndromic disorders caused by gain-of-function variants in KCNH1, KCNK4, and KCNN3-a subgroup of K(+) channelopathies.*Eur J Hum Genet.* 2021, 29: 1384-1395 http://dx.doi.org/10.1038/s41431-021-00818-9.
[8]Renart, M.L., *et al.* Modulation of Function, Structure and Clustering of K(+) Channels by Lipids: Lessons Learnt from KcsA.*Int J Mol Sci.* 2020, 21: http://dx.doi.org/10.3390/ijms21072554.
[9]Zhou, Y., *et al.* Chemistry of ion coordination and hydration revealed by a K+ channel-Fab complex at 2.0 A resolution.*Nature.* 2001, 414: 43-8 http://dx.doi.org/10.1038/35102009.
[10]Molina, M.L., *et al.* Influence of C-terminal protein domains and protein-lipid interactions on tetramerization and stability of the potassium channel KcsA.*Biochemistry.* 2004, 43: 14924-31 http://dx.doi.org/10.1021/bi048889+.
[11]Blasic, J.R., *et al.* Pore hydration states of KcsA potassium channels in membranes.*J Biol Chem.* 2015, 290: 26765-75 http://dx.doi.org/10.1074/jbc.M115.661819.
[12]Ryan, M.J., *et al.* Probing Ion Configurations in the KcsA Selectivity Filter with Single-Isotope Labels and 2D IR Spectroscopy.*J Am Chem Soc.* 2023, 145: 18529-18537 http://dx.doi.org/10.1021/jacs.3c05339.
[13]Giudici, A.M., *et al.* Tetraoctylammonium, a Long Chain Quaternary Ammonium Blocker, Promotes a Noncollapsed, Resting-Like Inactivated State in KcsA.*Int J Mol Sci.* 2021, 22: http://dx.doi.org/10.3390/ijms22020490.
[14]Lenaeus, M.J., *et al.* Structures of KcsA in complex with symmetrical quaternary ammonium compounds reveal a hydrophobic binding site.*Biochemistry.* 2014, 53: 5365-73 http://dx.doi.org/10.1021/bi500525s.
[15]Camagay, A.V., *et al.* Quaternary Ammonium Compound Toxicity. 2023: http://dx.doi.org/NBK594254 [bookaccession].
[16]Mohapatra, S., *et al.* Quaternary ammonium compounds of emerging concern: Classification, occurrence, fate, toxicity and antimicrobial resistance.*J Hazard Mater.* 2023, 445: 130393 http://dx.doi.org/10.1016/j.jhazmat.2022.130393.
[17]Faraldo-Gomez, J.D., *et al.* Mechanism of intracellular block of the KcsA K+ channel by tetrabutylammonium: insights from X-ray crystallography, electrophysiology and replica-exchange molecular dynamics simulations.*J Mol Biol.* 2007, 365: 649-62 http://dx.doi.org/10.1016/j.jmb.2006.09.069.
[18]Poveda, J.A., *et al.* Lipid modulation of ion channels through specific binding sites.*Biochim Biophys Acta.* 2014, 1838: 1560-7 http://dx.doi.org/10.1016/j.bbamem.2013.10.023.
[19]Renart, M.L., *et al.* Anionic Phospholipids Shift the Conformational Equilibrium of the Selectivity Filter in the KcsA Channel to the Conductive Conformation: Predicted Consequences on Inactivation.*Biomedicines.* 2023, 11: http://dx.doi.org/10.3390/biomedicines11051376.
[20]Triano, I., *et al.* Occupancy of nonannular lipid binding sites on KcsA greatly increases the stability of the tetrameric protein.*Biochemistry.* 2010, 49: 5397-404 http://dx.doi.org/10.1021/bi1003712.
[21]Poveda, J.A., *et al.* Modulation of the potassium channel KcsA by anionic phospholipids: Role of arginines at the non-annular lipid binding sites.*Biochim Biophys Acta Biomembr.* 2019, 1861: 183029 http://dx.doi.org/10.1016/j.bbamem.2019.183029.
[22]Poveda, J.A., *et al.* Towards understanding the molecular basis of ion channel modulation by lipids: Mechanistic models and current paradigms.*Biochim Biophys Acta Biomembr.* 2017, 1859: 1507-1516 http://dx.doi.org/10.1016/j.bbamem.2017.04.003.
[23]Zahra, A., *et al.* Identifying the mechanism of action of the Kv7 channel opener, retigabine in the treatment of epilepsy.*Neurol Sci.* 2023, 44: 3819-3825 http://dx.doi.org/10.1007/s10072-023-06955-x.
[24]Vigil, F.A., *et al.* Acute Treatment with the M-Channel (K(v)7, KCNQ) Opener Retigabine Reduces the Long-Term Effects of Repetitive Blast Traumatic Brain Injuries.*Neurotherapeutics.* 2023, 20: 853-869 http://dx.doi.org/10.1007/s13311-023-01361-9.
[25]Splinter, M.Y. Ezogabine (retigabine) and its role in the treatment of partial-onset seizures: a review.*Clin Ther.* 2012, 34: 1845-56 e1 http://dx.doi.org/10.1016/j.clinthera.2012.07.009.
[26]Shantha, G., *et al.* Role of dofetilide in patients with ventricular arrhythmias.*J Interv Card Electrophysiol.* 2023: http://dx.doi.org/10.1007/s10840-023-01578-w.
[27]Chen, C., *et al.* Efficacy and safety of dofetilide and sotalol in patients with hypertrophic cardiomyopathy.*Commun Med (Lond).* 2023, 3: 99 http://dx.doi.org/10.1038/s43856-023-00315-8.
[28]McClellan, K.J. and Markham, A. Dofetilide: a review of its use in atrial fibrillation and atrial flutter.*Drugs.* 1999, 58: 1043-59 http://dx.doi.org/10.2165/00003495-199958060-00007.
[29]Cicirale, C., *et al.* Safety of Inpatient Dofetilide Initiation per Cardiology Services: A Retrospective Review.*J Pharm Pract.* 2022, 35: 593-598 http://dx.doi.org/10.1177/08971900211000212.
[30]Lee, R.D., *et al.* Repurposing the K(Ca)3.1 Blocker Senicapoc for Ischemic Stroke.*Transl Stroke Res.* 2023: http://dx.doi.org/10.1007/s12975-023-01152-6.
[31]Zuccolini, P., *et al.* IK Channel-Independent Effects of Clotrimazole and Senicapoc on Cancer Cells Viability and Migration.*Int J Mol Sci.* 2023, 24: http://dx.doi.org/10.3390/ijms242216285.
[32]Bello-Perez, M. and Coll, J.M. Ligands docking to ORF8 by co-evolution. Could they reduce the inflammation levels induced by SARS-COV-2 infections?*ChemRxiv.* 2023, https://chemrxiv.org/engage/chemrxiv/article-details/655f2f3629a13c4d47ced2aa: http://dx.doi.org/10.26434/chemrxiv-2023-6r8s7.
[33]Bryant, P., *et al.* Structure prediction of protein-ligand complexes from seqeunce information with Umol.*bioRxiv.* 2023: http://dx.doi.org/10.1101/2023.11.03.565471.
[34]Coll, J.M. Evolutionary-docking targeting bacterial FtsZ.*ChemRxiv.* 2023, https://chemrxiv.org/engage/chemrxiv/article-details/6405c36fcc600523a3bcb679: http://dx.doi.org/10.26434/chemrxiv-2023-ld9d3
[35]Coll, J.M. Exploring non-toxic co-evolutionary docking.*ChemRxiv.* 2023, https://chemrxiv.org/engage/chemrxiv/article-details/6512b162ade1178b2424c325: http://dx.doi.org/10.26434/chemrxiv-2023-rr5b0.
[36]Bello-Perez, M., *et al.* SARS-CoV-2 ORF8 accessory protein is a virulence factor.*mBio.* 2023, 14: e0045123 http://dx.doi.org/10.1128/mbio.00451-23.
[37]Coll, J. Star-shaped Triazine-derivatives: would they crossbind SARS-CoV-2 spike helices?*ChemRxiv.* 2021, https://chemrxiv.org/engage/chemrxiv/article-details/6133c1096563696d9d222bbd: http://dx.doi.org/10.33774/chemrxiv-2021-xb6sx-v2.
[38]Lorenzo, M.M., *et al.* Would it be possible to stabilize prefusion SARS-COV-2 spikes with ligands?*ChemRxiv.* 2021: http://dx.doi.org/10.26434/chemrxiv.13453919.v2.
[39]Bermejo-Nogales, A., *et al.* Computational ligands to VKORC1s and CYPs. Could they predict new anticoagulant rodenticides?*BioRxiv.* 2021: http://dx.doi.org/10.1101/2021.01.22.426921.
[40]Dallakyan, S. and Olson, A.J. Small-molecule library screening by docking with PyRx.*Methods Mol Biol.* 2015, 1263: 243-50 http://dx.doi.org/10.1007/978-1-4939-2269-7_19.
[41]Morris, G.M., *et al.* AutoDock4 and AutoDockTools4: Automated docking with selective receptor flexibility.*J Comput Chem.* 2009, 30: 2785-91 http://dx.doi.org/10.1002/jcc.21256.
[42]Huey, R., *et al.* A semiempirical free energy force field with charge-based desolvation.*J Comput Chem.* 2007, 28: 1145-52 http://dx.doi.org/10.1002/jcc.20634.
[43]Trott, O. and Olson, A.J. AutoDock Vina: improving the speed and accuracy of docking with a new scoring function, efficient optimization, and multithreading.*J Comput Chem.* 2010, 31: 455-61 http://dx.doi.org/10.1002/jcc.21334.
[44]Coll, J. Could Acinetobacter baumannii Lol-abaucin docking be improved?*ChemRxiv.* 2023, https://chemrxiv.org/engage/chemrxiv/article-details/649aa71aba3e99daef1d1756: http://dx.doi.org/10.26434/chemrxiv-2023-962ht.
[45]Coll, J.M. New star-shaped ligands generated by evolutionary fitting the Omicron spike inner-cavity.*ChemRxiv.* 2023, https://chemrxiv.org/engage/chemrxiv/article-details/6479b8cfbe16ad5c57577cce: http://dx.doi.org/10.26434/chemrxiv-2023-v8gqj
[46]Coll, J.M. Anticoagulant rodenticide novel candidates predicted by evolutionary docking.*ChemRxiv.* 2023, https://chemrxiv.org/engage/chemrxiv/article-details/6479b8cfbe16ad5c57577cce: http://dx.doi.org/10.26434/chemrxiv-2023-gh4xl-v2.